J. Fluid Mech. (2012), *vol.* 710, *pp.* 131–153.
doi:10.1017/jfm.2012.354

Linear global instability of non-orthogonal incompressible swept attachment-line boundary-layer flow

José Miguel Pérez[1]†, Daniel Rodríguez[1,2] and Vassilis Theofilis[1]

[1] School of Aeronautics, Universidad Politécnica de Madrid, Plaza del Cardenal Cisneros 3, E-28040 Madrid, Spain

[2] Engineering and Applied Sciences, California Institute of Technology, Pasadena, CA 91125, USA

(Received 1 February 2012; revised 11 May 2012; accepted 4 July 2012; first published online 23 August 2012)

Flow instability in the non-orthogonal swept attachment-line boundary layer is addressed in a linear analysis framework via solution of the pertinent global (BiGlobal) partial differential equation (PDE)-based eigenvalue problem. Subsequently, a simple extension of the extended Görtler–Hämmerlin ordinary differential equation (ODE)-based polynomial model proposed by Theofilis *et al.* (2003) for orthogonal flow, which includes previous models as special cases and recovers global instability analysis results, is presented for non-orthogonal flow. Direct numerical simulations have been used to verify the analysis results and unravel the limits of validity of the basic flow model analysed. The effect of the angle of attack, AoA, on the critical conditions of the non-orthogonal problem has been documented; an increase of the angle of attack, from $AoA = 0$ (orthogonal flow) up to values close to $\pi/2$ which make the assumptions under which the basic flow is derived questionable, is found to systematically destabilize the flow. The critical conditions of non-orthogonal flows at $0 \leqslant AoA \leqslant \pi/2$ are shown to be recoverable from those of orthogonal flow, via a simple algebraic transformation involving AoA.

Key words: BiGlobal, stability, attachment-line

1. Introduction

Plane stagnation flows are commonly employed models to describe flow in the vicinity of the leading edge of cylinders and aerofoils in the limit of vanishing curvature. Plane stagnation point flow, formed when a uniform flow impinges on a flat plate at right angles to the surface, is described by the classic (orthogonal, unswept) Hiemenz (1911) boundary layer, which is an exact solution of the incompressible continuity and Navier–Stokes equations (Schlichting 1979). Customarily, Hiemenz flow is defined on the plane Oxy, where x is the chordwise and y is the wall-normal spatial direction, the free-stream velocity component being $-V_\infty$, as schematically depicted in figure 1. Stagnation line flow arises when a constant free-stream velocity component, W_∞, is also introduced along the spanwise direction, represented by the z-axis in figure 1 and resulting in a fully three-dimensional boundary layer, which

† Email address for correspondence: jomipp@torroja.dmt.upm.es

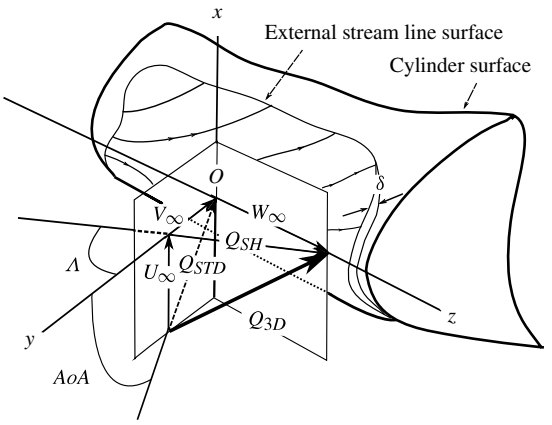

FIGURE 1. Schematic representation of the non-orthogonal swept attachment-line boundary-layer flow where Q_{STD} is the potential flow velocity vector discussed by Stuart (1959), Tamada (1979) and Dorrepaal (1986), Q_{SH} is that used by Hall *et al.* (1984), while Q_{3D} is that corresponding to the general case discussed herein.

is also an exact solution of the incompressible equations of motion. This so-called infinite swept attachment-line boundary-layer flow is widely accepted as a model describing incompressible flow in the vicinity of the windward face of swept cylinders and aerofoils at high Reynolds numbers (Rosenhead 1963). The limitations of this flow model are encountered when compressibility or curvature are introduced. Stagnation line flow, in which the sweep angle Λ may be defined through the external free-stream velocity components, $\Lambda \equiv \arctan(W_\infty/V_\infty)$, is antisymmetric as far as the chordwise boundary-layer velocity component is concerned, and symmetric as regards the wall-normal and spanwise velocity components inside the boundary layer. The symmetry of orthogonal plane stagnation flows is broken when a non-zero chordwise free-stream velocity component U_∞ exists and defines the angle of attack, $AoA \equiv \arctan(U_\infty/V_\infty)$. Non-orthogonal stagnation point flow, defined by the existence of $U_\infty, V_\infty \neq 0$ and $W_\infty = 0$, has independently been rediscovered in a space of 30 years by Stuart (1959), Tamada (1979) and Dorrepaal (1986), and will be referred to as STD flow in what follows. Non-orthogonal stagnation-line flow arises on account of three non-zero free-stream velocity components, $U_\infty, V_\infty, W_\infty \neq 0$, as schematically shown in figure 1. A compressible non-orthogonal stagnation-line flow model valid at small Mach numbers has been first presented by Lasseigne & Jackson (1992). More realistic models of boundary-layer flow in the vicinity of swept leading edges have been studied by Lin & Malik (1997), who introduced curvature effects in the incompressible orthogonal swept attachment-line boundary layer, while compressible laminar steady states pertinent to orthogonal stagnation flows have been obtained by direct numerical simulation (DNS) in the neighbourhood of swept cylinders of circular (Collis & Lele 1999), elliptic (Xiong & Lele 2007) and parabolic (Mack, Schmid & Sesterhenn 2008) cross-sections.

The vast majority of both theoretical and experimental work as regards instability of plane stagnation flows has been performed in the orthogonal limit. In the following discussion we only summarize facts related to the present work; an extensive discussion may be found in Pérez (2012). Early experimentation (Gray 1952) detected boundary-layer transition on swept wings with laminar aerofoils, which was found to move toward the attachment-line direction when the sweep angle was increased.

The associated instability was attributed to a cross-flow mechanism (Gaster 1967; Pfenninger & Bacon 1969) while Poll (1979) postulated that there exists a clear distinction between attachment-line and cross-flow instabilities, for which viscous and inviscid processes are responsible, respectively. In addition, in the experiments of both Pfenninger & Bacon (1969) and Poll (1979) a critical Reynolds number, $Re \approx 245$, was obtained when finite-amplitude perturbations were used to drive the transition process. This value corresponds to the lowest value of the Reynolds number below which no linear instability exists (see Joslin 1996). Modelling of attachment-line instability in the limit of orthogonal stagnation point flow, $AoA = \Lambda = 0$, commenced with the classic works of Görtler (1955) and Hämmerlin (1955). These authors postulated that linear perturbations inherit the symmetries of the basic flow, for which the chordwise velocity component inside the boundary layer is a linear function of the chordwise coordinate, while the wall-normal perturbation velocity component is only a function of the wall-normal spatial coordinate. A stable mode was obtained with this formulation. Later, Wilson & Gladwell (1978) showed that there exist two types of linear stability modes in stagnation point flow; those that decay algebraically in the wall-normal direction and others that decay exponentially. They argued that the former disturbances must be excluded for physicals reasons and showed that exponentially decaying modes are always stable, in line with the earlier predictions. Still within the realm of linear theory, Brattkus & Davis (1991) discussed an expansion of arbitrary disturbances in Hermite polynomials of the chordwise coordinate; they obtained linear stable flows in which the modes postulated by Görtler–Hämmerlin (GH) were the least damped. Finally, Lyell & Huerre (1985) addressed both linear and nonlinear instability of plane stagnation point flow and showed that, while linearly stable this flow can become nonlinearly unstable to three-dimensional perturbations, a result which was later corroborated in the DNS of Spalart (1988). Regarding linear instability of orthogonal plane stagnation line flow, the work of Hall, Malik & Poll (1984) extended the unswept Hiemenz basic flow model for stagnation point flow to incorporate a constant spanwise velocity component. The GH model for the linear perturbations, extended to the third, spanwise perturbation velocity component was incorporated in the analysis, which showed that the incompressible stagnation line flow becomes linearly unstable for a critical Reynolds number $Re \approx 583.1$, a result confirmed experimentally in the same work and also by solving the initial-value problem for linear perturbations (Theofilis 1993); work in this context was completed by the solution of the corresponding spatial stability eigenvalue problem (EVP) (Theofilis 1995). Criminale, Jackson & Lasseigne (1994), recognizing the impossibility of treating the stability problem by normal modes having one-dimensional amplitude functions in the general case in which no special structure on their dependence on the spatial coordinates is assumed, also addressed the initial-value problem in the inviscid limit; they found that two-dimensional plane stagnation flow is stable, as opposed to its three-dimensional counterpart in which linear instability may develop. The first three-dimensional DNS of incompressible stagnation-line flow by Spalart (1988) delivered a number of important results. First, stagnation-point flow was found to be nonlinearly stable. Second, the GH structure of the most unstable eigenmodes was recovered in a DNS initialized by noise. Finally, finite-amplitude perturbations delivered a critical Reynolds number of $Re \approx 245$, that is substantially lower than that delivered by linear stability theory. In this manner, both the experimental results of Pfenninger & Bacon (1969) and Poll (1979) and the theoretical predictions of Lyell & Huerre (1985) regarding nonlinear instability of unswept flow were fully confirmed.

Global linear instability analysis was also first performed in the orthogonal limit. Lin & Malik (1996) were the first to go beyond the apparently restrictive GH Ansatz assumption and perform a modal linear stability analysis of the incompressible stagnation-line flow without being conditioned by this hypothesis. The leading GH eigenmodes of the earlier local analyses were recovered as the most amplified global modes, while additional eigenmodes were discovered, which are less amplified than that discovered by Hall *et al.* (1984). Lin & Malik (1997) went on to analyse by global linear stability theory the effect of streamwise curvature and concluded that it stabilizes the flow, thus offering additional motivation to analyse the stability of plane stagnation flows first. Theofilis *et al.* (2003) also performed global instability analysis and DNS of the incompressible swept Hiemenz flow, fully confirming the existence of the sequence of the global modes predicted by Lin & Malik (1996), and proposed a polynomial model to describe the chordwise dependence of the amplitude functions of these modes. The polynomial model converts the partial differential equation (PDE)-based global linear instability analysis EVP into an ordinary differential equation (ODE)-based one, without loss of physical information in the linear regime. Bertolotti (1999) dealt with the problem of connection between attachment-line instabilities and stationary cross-flow vortices, the latter observed in the DNS of Spalart (1988), using a parabolized stability equations formulation, and showed that these two classes of disturbances are connected to each other. Recently Mack *et al.* (2008), using DNS-based global stability analysis of the compressible swept leading-edge flow around a parabolic body, confirmed that a connection between attachment-line and cross-flow modes exists also in compressible flow. Evidence is thus amassed against the separation between attachment-line and stationary cross-flow modes, postulated in earlier descriptions of stagnation-line flow instabilities. The global instability analysis problem in compressible swept attachment-line boundary-layer flow was first solved by Theofilis, Fedorov & Collis (2006), who also presented an ODE-based EVP model, the results of which compared favourably with the global EVP solutions in the subsonic regime. More recently, Mack *et al.* (2008) and Mack & Schmid (2010) studied the global stability of flow in the leading-edge region of a swept blunt cylindrical body of infinite span in compressible flow using DNS-based global stability analysis. As well as confirming the connection between attachment-line and cross-flow modes, these authors also identified acoustic branches of instability and found evidence of the presence of non-modal instability effects in compressible orthogonal stagnation-line flows.

Finally, receptivity and non-modal linear instability analyses have also been performed in the orthogonal stagnation line flow limit. Receptivity has been addressed by Floryan & Dallmann (1990), who studied the effect of wavy-surface roughness on linear amplification of modal perturbations satisfying the GH Ansatz in incompressible flow and found that this type of roughness generates streamwise vorticity. Xiong & Lele (2007), building upon and extending the vorticity amplification theory of Sutera (1965), addressed the effect of length scales of free-stream turbulence on the distortion and linear amplification of unsteady disturbances inside the swept Hiemenz boundary layer, and arrived at a parameter relating the free-stream and the inherent boundary-layer scales as being the determining parameter to describe this phenomenon. Collis & Lele (1999) also investigated surface roughness, but concentrated on its effect in a region of a parabolic cylinder body where stationary cross-flow vortices are generated and showed that curvature and non-parallel effects were the major counteracting competitive mechanisms in order to predict the initial amplitude of the stationary cross-flow vortices. Non-modal effects of incompressible stagnation line

flows were addressed in several efforts during the last decade. Obrist & Schmid (2003) showed that the modes predicted by linear stability theory can exhibit strong transient growth for polynomial orders higher than zero, while Guégan, Schmid & Huerre (2008) identified optimal disturbances for the spatial stability problem.

Substantially less is known regarding stability of the non-orthogonal stagnation flows. In the incompressible regime Floryan (1992) introduced a perturbation model satisfying an extension of the GH Ansatz to describe linear stability of the (stagnation point) STD flow, as well as a class of perturbations which did not assume this Ansatz; he found both classes to be linearly stable. Lasseigne & Jackson (1992) employed local theory to the compressible non-orthogonal stagnation line problem at low Mach and constant Prandtl numbers in order to investigate temperature and suction effects near the attachment line. These authors proposed a self-similarity solution for the basic flow based on the STD model, and used the GH Ansatz to describe the most unstable modal perturbations. Although *a priori* the presence of $AoA \neq 0$ prohibits the imposition of symmetries along the chordwise direction, an angle-independent version of the stability system was recovered by a suitable scaling with the angle of attack. In subsequent work Lasseigne, Jackson & Hu (1992) used the same basic flow model to study the effect of suction and heat transfer on the stagnation line region and found that suction and cooling stabilizes the flow, while to the opposite effect is caused by blowing and heating.

The present contribution addresses the following open issues in incompressible stagnation-line flow. First, a model for the basic state describing this flow is derived. This model is an extension of the STD flow and is identical with that proposed by Lasseigne & Jackson (1992), if the limit of zero Mach number is taken in the latter work. Second, stability of incompressible non-orthogonal stagnation line flows is addressed from a global modal linear instability analysis perspective, by solving the BiGlobal EVP pertinent to this flow for the first time, in order to study the effect of the angle of attack on the known linear stability results of swept Hiemenz flow, as well as on those of plane non-orthogonal stagnation-point flow (Floryan 1992). Third, in the spirit of earlier work on the plane stagnation-line flow, an ODE model is derived to describe the instability of plane non-orthogonal stagnation-line flow. It includes and extends the models of Floryan (1992) and of Lasseigne & Jackson (1992) in the incompressible limit, and is shown to recover the instability results offered by the solution of the partial-derivative EVP, at a fraction of the cost of the latter, without loss of physical information. Parametric studies varying the Reynolds number and the spanwise wavenumber at several discrete values of $0 \leqslant AoA \leqslant \pi/2$ have been used to obtain the neutral values of non-orthogonal flows as a function of angle of attack. All EVP results are validated by DNSs and demonstrate destabilization of the flow with increasing angle of attack, up to the highest values of the latter parameter examined. Finally, the critical conditions of non-orthogonal plane stagnation flow are related with those of its orthogonal counterpart by a simple algebraic transformation.

The STD basic flow model is extended to include sweep and solved in § 2. The equations governing the global linear stability problem are derived and solved in § 3. Validation results, obtained independently by DNS, are also obtained in this section. Section 4 presents the polynomial model which recovers the global instability analysis results of § 3, as well as the neutral curves as a function of the angle of attack. Based on the observations made on the preceding sections, § 4.2 proposes a theoretical scaling of the instability results with the angle of attack. A short discussion in § 5 closes the presentation.

2. Problem definition and basic flow computation

A schematic representation of the problem geometry and the incoming flow conditions are shown in figure 1. The x-axis is taken to be along the chordwise spatial direction, y is the normal direction to the body surface and the z-axis is along the spanwise direction. No pressure gradients are present along the spanwise direction, and the effect of wall curvature is neglected. The oblique potential flow vector, $\boldsymbol{Q}_{3D}$, far from the wall has a constant component W_∞ in the spanwise direction, while its direction is defined by the angles $\Lambda \equiv \arctan(W_\infty/V_\infty)$ and $AoA \equiv \arctan(U_\infty/V_\infty)$.

A similarity solution is proposed here for oblique stagnation-line flow with a sweep component. This model is based on the solution for the (two-dimensional) unswept problem ($W_\infty = 0$) that was independently proposed by Stuart (1959) and Tamada (1979) and, in a most complete form, by Dorrepaal (1986). Common to all three works is the consideration of a linear combination of orthogonal stagnation and shear flows. Under this assumption, the two-dimensional streamfunction is decomposed into a normal component corresponding to the Hiemenz solution describing the orthogonal limit (Hiemenz 1911) and a tangential component:

$$\psi(x, y) = x\nu f(y) + \nu g(y), \tag{2.1}$$

where x and y are dimensionless variables scaled by $\Delta = (\nu/S)^{1/2}$, ν is the kinematic viscosity and $S = (\partial U_e/\partial x)_{x=0}$ is the local strain rate at the boundary layer of the orthogonal basic flow. The tangential and normal velocity components are then obtained from

$$u(x, y) = xS\Delta f'(y) + S\Delta g'(y), \quad v(y) = -S\Delta f(y). \tag{2.2}$$

Note that the non-orthogonality only affects the tangential velocity component, while the wall-normal velocity is formally identical with that of the orthogonal flow. A spanwise velocity component is introduced when $W_\infty \neq 0$. It is assumed that the spanwise velocity component depends only on the wall-normal direction y. Scaling velocities with W_∞, the Reynolds number $Re = W_\infty \Delta/\nu$ is introduced and, in a manner consistent with the orthogonal swept stagnation line formulation, the complete form of the basic flow is written as

$$U(x, y) = \frac{x}{Re} f'(y) + \frac{1}{Re} g'(y), \quad V(y) = -\frac{1}{Re} f(y), \quad W(y) = \bar{w}(y). \tag{2.3}$$

Introducing these expressions into the Navier–Stokes momentum equations, since continuity is satisfied by definition (see (2.2)) delivers the following system of ODEs.

Normal component:

$$f'''(y) + f(y)f''(y) - f'(y)^2 + \sin(\alpha)^2 = 0, \tag{2.4a}$$

$$f(0) = f'(0) = 0, \quad f'(\infty) = \sin(\alpha). \tag{2.4b}$$

Tangential component:

$$g'''(y) + f(y)g''(y) - f'(y)g'(y) + A\sin(\alpha)^{1/2}\cos(\alpha) = 0, \tag{2.5a}$$

$$g(0) = g'(0) = 0, \quad g''(\infty) = \cos(\alpha). \tag{2.5b}$$

Spanwise component:

$$\bar{w}''(y) + f(y)\bar{w}'(y) = 0 \tag{2.6a}$$

$$\bar{w}(0) = 0, \quad \bar{w}(\infty) = 1. \tag{2.6b}$$

In the previous expressions, primes denote differentiation with respect to y, $A \approx 0.647900$ is the displacement thickness (Dorrepaal 1986) and $(-2\tan\alpha)$ is the

slope of the streamline $\psi = 0$ on the outer potential flow. In the limit $\alpha = \pi/2$ the well-known swept Hiemenz flow is obtained. The angle of attack AoA and the angle α are related via,

$$AoA = \tan^{-1}(-2\tan\alpha) + \frac{\pi}{2}. \tag{2.7}$$

An angle-independent version of the system (equations (2.4)–(2.6)) can be recovered by introducing the scaled wall-normal variable $\eta = ay$, where $a = \sqrt{\sin\alpha}$, and the following change of variables,

$$f(y) = aF(\eta), \tag{2.8a}$$

$$g'(y) = \frac{\cos\alpha}{a}H(\eta), \tag{2.8b}$$

$$\bar{w}(y) = E(\eta). \tag{2.8c}$$

The resulting system of equations for the basic flow, independent of α, is

$$F'''(\eta) + F(\eta)F''(\eta) - F'(\eta)^2 + 1 = 0, \tag{2.9a}$$

$$F(0) = F'(0) = 0, \quad F'(\infty) = 1. \tag{2.9b}$$

$$H''(\eta) + F(\eta)H'(\eta) - F'(\eta)H(\eta) + A = 0, \tag{2.9c}$$

$$H(0) = 0, \quad H'(\infty) = 1. \tag{2.9d}$$

$$E''(\eta) + F(\eta)E'(\eta) = 0, \tag{2.9e}$$

$$E(0) = 0, \quad E(\infty) = 1. \tag{2.9f}$$

The relative scale factors of normal and tangential components can be obtained by replacing the previous equations on (2.2) and taking the limit for large y. Therefore, the tangential component is scaled by $S\sin\alpha$ and the normal component is scaled by $S\cos\alpha$.

The ODE system governing the basic flow (equations (2.4)–(2.6)) was solved numerically using a shooting method. Estimates for the second derivatives of functions f and g at the wall are required, and can be obtained from the asymptotic expressions of f and g for small y: $f''(0) = C\sin(\alpha)^{3/2}$ and $g''(0) = D\cos\alpha$, where $C = 1.232588 = f''(0)_{\alpha=\pi/2}$ and $D = 1.406544$, as discussed by Dorrepaal (1986). The shooting method was used to obtain solutions between the wall and a relatively large value of y, where the functions have reached their asymptotic behaviour; the latter are then extended analytically until the end of the computational domain. Extensive validation of the basic flow has been performed, including the recovery of the orthogonal swept Hiemenz basic flow in the limit of $\alpha = \pi/2$ and asymptotic results provided by Dorrepaal (1986) at small and large y values. The location of the stagnation point on the xy plane for different values of α was computed as a validation check. As demonstrated by Dorrepaal (1986), the stagnation point shifts from $x = 0$ towards the direction of the incoming flow as the angle α decreases from $\alpha = \pi/2$. The stagnation point location obtained numerically by the present algorithm is compared in table 1 with the theoretical values of the reference work at different values of the angle α. The streamlines and isocontours plot of wall-normal velocity component are presented in figures 2(*a*) and 2(*b*) for two different angles, namely $\alpha = \pi/2$ and $\alpha = \pi/3$.

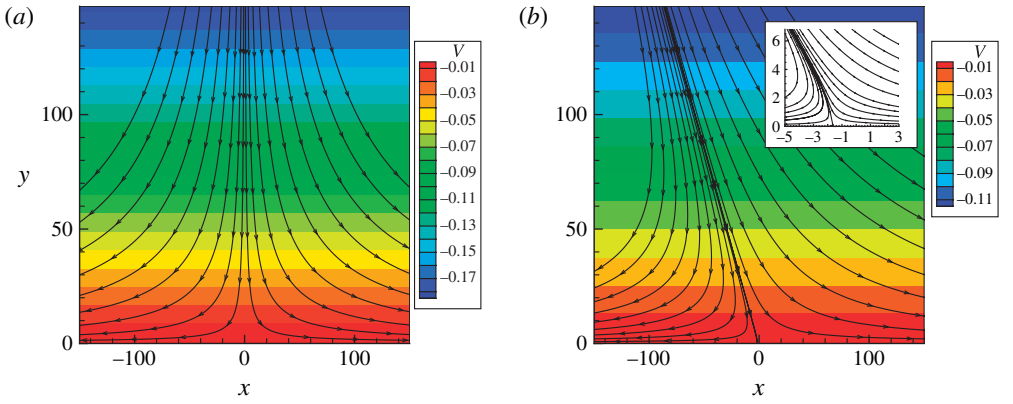

FIGURE 2. (Colour online) Streamlines and normal velocity component of the basic flow at two angles: (*a*) $\alpha = \pi/2$ (orthogonal flow) and (*b*) $\alpha = \pi/3$. The displacement of the stagnation point is shown in the inset of panel (*b*). This displacement shift corresponds to the value corresponding value presented in table 1.

α (deg.)	Present results	Dorrepaal (1986)
70	0.426	0.429
50	1.089	1.094
30	2.793	2.795

TABLE 1. Comparison of the present basic flow solution against the reference work of Dorrepaal (1986). Shown is the streamwise coordinate x of the streamline $\psi = 0$.

3. Three-dimensional linear instability analysis of non-orthogonal plane stagnation-line flow

Two complementary methodologies for the analysis of linear instability are employed, namely a partial-derivative-based EVP, usually referred to as the BiGlobal instability problem, and DNSs. The independence of the instability results on the methodology employed is used as cross-validation. Temporal linear stability analysis considers the evolution of small-amplitude perturbations superposed upon a steady basic flow. The smallness of the perturbations permits the linearization of the Navier–Stokes equations around the reference basic flow, neglecting the second-order nonlinearities between the perturbation components. Linear instability analysis for the present problem considers a three-component basic flow velocity vector (2.3) which is inhomogeneous in two out of the three spatial directions, i.e. no dependence exists on the spanwise coordinate z. This permits the introduction of Fourier modes in order to describe the behaviour of the perturbations along the z-direction. In the context of a linear analysis, the individual spanwise modes, characterized by the wavenumber $\beta = 2\pi/L_z$ with L_z a spanwise wavelength, are mutually independent and the linear stability problem can be studied for each β separately.

3.1. *BiGlobal modal linear instability theory*

The BiGlobal instability EVP, as described in detail by Theofilis (2003, 2011), is applied here to the problem at hand. The general solution of the equations of motion is

decomposed as

$$\boldsymbol{Q}(x, y, z, t) = \boldsymbol{Q}_b(x, y) + \epsilon \,\mathrm{Re}\left\{\boldsymbol{Q}_p(x, y) \exp\left(\mathrm{i}\left(\beta z - \Omega t\right)\right)\right\}, \tag{3.1}$$

where $\boldsymbol{Q}_b(x, y) = (U, V, W)$ is the basic flow defined in (2.3), $\boldsymbol{Q}_p(x, y) = \left(\hat{u}, \hat{v}, \hat{w}, \hat{p}\right)(x, y)$ is the vector of two-dimensional disturbance amplitude functions, $\epsilon \ll 1$ is the amplitude of the perturbation and Ω a complex frequency: $\mathrm{Re}\{\Omega\}$ and $\mathrm{Im}\{\Omega\}$ are the phase velocity and the growth or damping rate of the perturbation, respectively. Substitution of the decomposition (3.1) into the incompressible continuity and Navier–Stokes equations and linearization around the basic state on account of the smallness of ϵ yields

$$\mathscr{D}_x\hat{u} + \mathscr{D}_x\hat{v} + \mathrm{i}\beta\hat{w} = 0, \tag{3.2}$$

$$\left[\mathscr{N} - (\mathscr{D}_x U)\right]\hat{u} - \left(\mathscr{D}_y U\right)\hat{v} - \mathscr{D}_x\hat{p} = -\mathrm{i}\Omega\hat{u}, \tag{3.3}$$

$$-\left(\mathscr{D}_y V\right)\hat{u} + \left[\mathscr{N} - \left(\mathscr{D}_y V\right)\right]\hat{v} - \mathscr{D}_y\hat{p} = -\mathrm{i}\Omega\hat{v}, \tag{3.4}$$

$$-\left(\mathscr{D}_x W\right)\hat{u} - \left(\mathscr{D}_y W\right)\hat{v} - \mathscr{N}\hat{w} - \mathrm{i}\beta\hat{p} = -\mathrm{i}\Omega\hat{w}. \tag{3.5}$$

where $\mathscr{N} = (1/Re)\left(\mathscr{D}_x^2 + \mathscr{D}_y^2 - \beta^2\right) - U\mathscr{D}_x - V\mathscr{D}_y - \mathrm{i}\beta\mathscr{W}$, $\mathscr{D}_x = \partial/\partial x$ and $\mathscr{D}_y = \partial/\partial y$. This system defines a two-dimensional generalized EVP for the temporal evolution of three-dimensional perturbations when complemented by appropriate boundary conditions. No-slip condition is imposed at the wall to the velocity components, along with a compatibility condition for the pressure. Vanishing of all the perturbation components is imposed in the far-field. Along the chordwise direction a linear extrapolation at $|x| \to \infty$ (Theofilis *et al.* 2003) and pressure compatibility conditions are imposed. More specifically, the second derivative of the disturbances along the chordwise direction was set equal to zero, $\partial^2\hat{q}/\partial x^2 = 0$. Although the application of these boundary conditions to unbounded flows often leads to the appearance of a numerical boundary layer in which the results are not physical, their effect can be minimized in two ways: (*a*) extending the computational domain, i.e. displacing the boundaries away from the stagnation point; and (*b*) increasing the resolution at the boundaries, e.g. by using a stretching function that clusters points in those regions. The values of the parameters used in the computations (size domain and number of points) were chosen after a study of convergence considering the two points exposed above. For these parameters, the amplitude functions of the more unstable modes, as well as their growth rates, are practically unaffected by the boundary conditions.

3.1.1. *Numerical solution, verification and validation*

The EVP (3.2)–(3.5) is discretized in a coupled manner using the Chebyshev–Gauss–Lobatto (CGL) collocation grid along both the x- and y-directions. A linear mapping of the CGL grid is used along the x-direction, while an algebraic mapping is used to cluster points in the vicinity of the wall with the aim of better resolving the strong gradients in the boundary layer; the details of the transformation are discussed by Theofilis *et al.* (2003). A spectral collocation method is used for the evaluation of the differentiation matrices inside of the linear operator. A shift-and-invert implementation of the Arnoldi algorithm is employed in order to recover a window of the eigenspectrum centred around the shift parameter σ. Consequently, the Arnoldi algorithm is applied to the problem

$$\hat{\boldsymbol{A}}X = \mu X \quad \text{where } \hat{\boldsymbol{A}} = (\boldsymbol{A} - \sigma\boldsymbol{B})^{-1}\boldsymbol{B}, \mu = \frac{1}{\Omega - \sigma}. \tag{3.6}$$

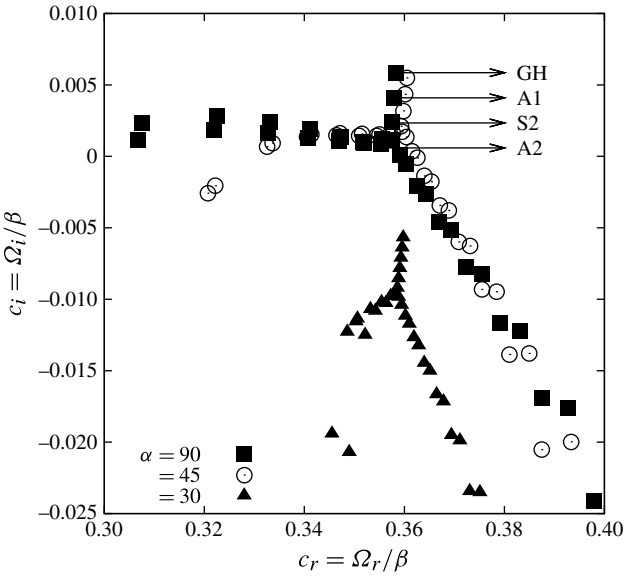

FIGURE 3. Typical spectra at $Re = 800$, $\beta = 0.255$ and three angles, $\alpha = 90°$ (orthogonal flow), $\alpha = 45°$ and $\alpha = 30°$.

The linear algebra work is performed using two alternatives, dense linear-algebra library routines and the sparse Multifrontal Massively Parallel Sparse direct Solver (MUMPS) package (Amestoy *et al.* 2001), the latter first successfully employed to global linear instability problems by Crouch, Garbaruk & Magidov (2007).

A first validation case of the present numerical solution is performed by revisiting the orthogonal case of Lin & Malik (1996) at $Re = 800$ and $\beta = 0.255$. Convergence of the eigenvalues is attained using 64 collocation nodes in either the chordwise and wall-normal directions, and a computational domain $x \in [-200, 200]$ and $y \in [0, 150]$. Changes in the domain length affect the eigenvalues beyond the seventh significant figure. Convergence of the leading eigenvalues is also attained using a domain smaller in the x-direction, as well as a smaller number of discretization points. However, a large domain in the x-direction eases the comparison with the direct numerical computations to be presented below in this section, and all subsequent computations in this paper are performed using this domain size. Further validations of the BiGlobal EVP are performed by comparing its results with those delivered by DNSs of the problem at hand. These validations are presented in §§3.3.1 and 3.3.2.

3.2. *Characteristics of the eigenspectrum and eigenfunctions*

Prior to comparing the linear instability results provided by the BiGlobal EVP and the DNS, it is instructive to expose some fundamental properties of the eigenspectrum and the corresponding eigenfunctions associated with the non-orthogonal swept attachment-line flow, as compared with their orthogonal counterparts.

Figure 3 shows the eigenspectrum corresponding to three different angles: $\alpha = 90°$ (orthogonal flow), $\alpha = 45°$ and $\alpha = 30°$ at a single set of parameters, $Re = 800$, $\beta = 0.255$. The orthogonal case is the same as that was used in the validation test discussed in § 3.1.1. An analogous eigenspectrum structure appears for any of the combinations of parameters examined. The leading family of eigenvalues that was identified in the case of orthogonal stagnation-line flow by Lin & Malik (1996),

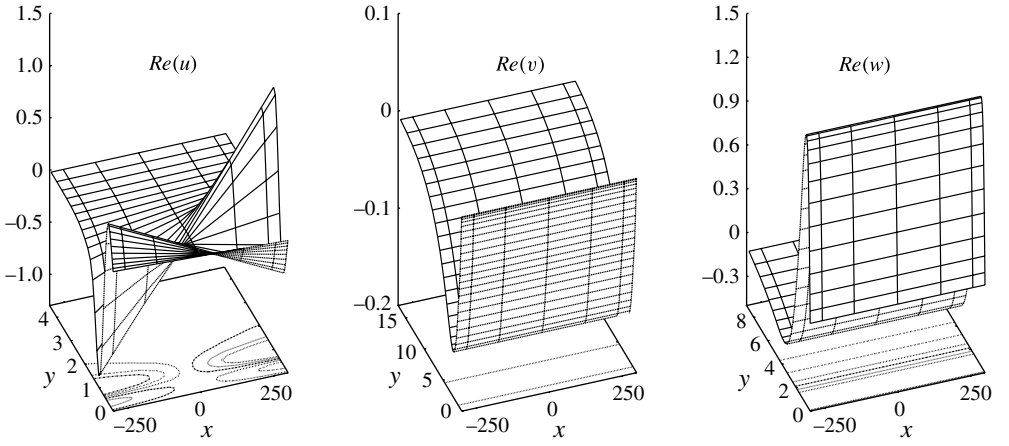

FIGURE 4. Perspective view of the real parts of the disturbance eigenfunctions of the GH linear eigenmode, as obtained by numerical solution of the BiGlobal EVP, corresponding to $Re = 800$, $\beta = 0.255$ at $\alpha = 45°$.

comprising symmetric (S1, S2, etc.) and antisymmetric modes (A1, A2, etc.), is also recovered here. In the case of non-orthogonal stagnation flow, the division of modes in symmetric and antisymmetric is not strictly applicable, as the symmetry properties are not preserved. However, the location of the eigenmodes in the spectra, as well as some qualitative properties of the eigenfunctions, can be traced from the orthogonal case as the angle α is decreased from $\alpha = 90°$ (or *AoA* increased from 0°), and therefore this notation will be preserved in what follows.

The first mode of this family was postulated by Görtler (1955) and Hämmerlin (1955) to have a linear dependence in the chordwise direction in the case of orthogonal flow, and is commonly referred to in the literature as the GH mode or the S1 mode. As is the case in orthogonal flow, the GH mode dominates at any parameter combination in the range analysed, and consequently neutral curves of the non-orthogonal flow may be obtained by reference to this eigenmode alone. Two additional branches of eigenmodes are present, but they are irrelevant to the linear modal instability, due to their stable behaviour. The splitting in the tail of the third eigenvalue branch, observable towards higher damping rates in figure 3, is known to be the result of finite-precision arithmetic and a fixed maximum permissible resolution on the hardware utilized.

In the orthogonal case, it was found that there is a relation between the position of a mode on its branch and the order of the polynomial model representing the amplitude function behaviour along the chordwise direction. This relation is not exact in the non-orthogonal case, i.e. eigenfunctions for mode GH are not exactly linear functions of x, but it serves as a first approximation, especially as $\alpha \to 90°$. Figure 4 shows the amplitude functions corresponding to the mode GH at $Re = 800$, $\beta = 0.255$, $\alpha = 45°$ highlighted in figure 3. The chordwise velocity component $\hat{u}$ is approximately linear with x and the other two velocity components, $\hat{v}$ and $\hat{w}$, are independent of this coordinate.

3.3. *Cross-validation of instability analysis results using DNS*

Verification and validation of the non-orthogonal global linear stability EVP is completed by comparisons against results delivered by DNSs, utilizing a spatial DNS

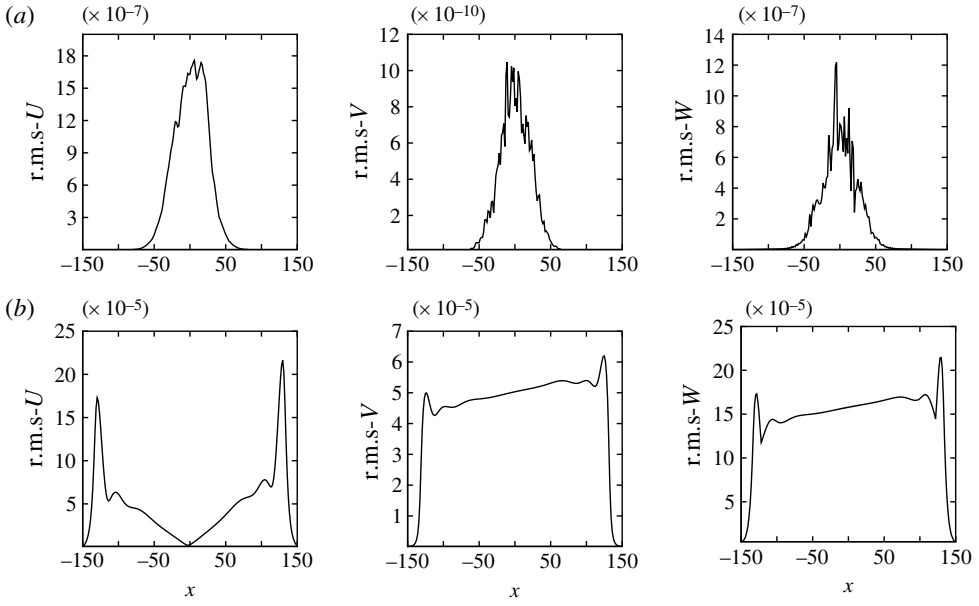

FIGURE 5. Maximum over y of the r.m.s. integrated over z of disturbance velocity components at $Re = 750$, $\beta = 0.25$ and $\alpha = 60°$, with (a) $t = 0$ and (b) $t = 7000$. Panel (b) is obtained by DNS from an initial noise (a).

code originally written by Lundbladh *et al.* (1994), as modified by Obrist (2000). The same approach has been successfully used in validating results in the orthogonal limit (Theofilis *et al.* 2003) where the modifications made in order to solve the problem at hand are described. Further modifications are necessary here in order to introduce a non-orthogonal basic flow. The computational domain $x \in [-150, 150]$, $y \in [0, 150]$ is considered, using $(192 \times 97 \times 16)$ collocation points along the x, y and z spatial directions, respectively. A fringe region extending 10 % of the chordwise domain extension is placed at each side of the computational domain to prevent reflections of the perturbations. Advective and diffusive Courant–Friedrichs–Lewy (CFL) numbers are taken equal to 0.08 and 0.5, respectively. Two test cases are considered, discussed in what follows.

3.3.1. *The Spalart test in non-orthogonal flow*

The most unstable linear perturbations are recovered from the temporal evolution of random perturbations superposed upon on the basic flow, at several combinations of the Reynolds number and wavenumber parameters, of which results at $Re = 1000$, $\beta = 0.2$, $\alpha = 60°$ are discussed in some detail next. Figure 5 shows the spatial development with x of the r.m.s. (root mean square of velocities integrated over z) of the velocity components pertaining to the leading eigenmode, after the introduction of noise at time $t = 0$. As can be seen, there exists a region around the stagnation point where the modal energy distribution of the most unstable mode is recovered from the initial noise perturbation. As seen in figure 4, the chordwise perturbation velocity component depends nearly linearly on x, while the other two velocity components are practically independent of x, as predicted by the classic Görtler–Hämmerlin Ansatz. Further discussion of this point will be offered in § 4.

α (deg.)	$c_{i,2D-EVP} \times 10^{-3}$	$c_{i,DNS} \times 10^{-3}$	Relative error (%)
80	4.636	4.624	0.26
70	5.292	5.292	0.01
60	6.052	6.060	0.13
50	6.236	6.296	0.96
40	4.336	4.324	0.28
30	−3.380	−3.356	0.71

TABLE 2. Growth rates of the leading GH eigenmode for oblique cases predicted by the BiGlobal linear stability theory, $c_{i,2D-EVP}$ and by DNS, $c_{i,DNS}$, for a range of angles. $\beta = 0.25$, $Re = 750$.

3.3.2. *Recovery of amplification rates*

The amplification or damping rate of modal perturbations may be obtained using the DNS code (e.g. Rodríguez & Theofilis 2010), through

$$\Omega_i = \frac{\ln E(\beta, t + \delta t) - \ln E(\beta, t)}{2\Delta t}, \tag{3.7}$$

where $E(\beta, t) = (1/2L') \int_0^{L_y} \mathrm{d}y \int_{-L'}^{L'} (1/2)\hat{\boldsymbol{u}}\hat{\boldsymbol{u}}\,\mathrm{d}x$ is the modal energy, $\hat{\boldsymbol{u}}$ is the disturbance velocity vector, L' is a streamwise domain extent, excluding the influence of the fringe region, and Δt the CFL-controlled time step.

Table 2 compares the growth rates of the leading GH eigenmode predicted by BiGlobal EVP $c_{i,2DEVP} = \Omega_{i,2DEVP}/\beta$ with those extracted from the DNS, $c_{i,DNS} = \Omega_{i,DNS}/\beta$, for $Re = 750$ and a variety of α values.

In these DNSs, the choice of the axial extent $L' = 200$ used in the chordwise direction was based on a convergence study for the growth rate and the amplitude functions while a spanwise extension of the domain $z \in [-8\pi, 8\pi]$ was employed in order to accommodate two periods of the fundamental wavelength associated with $\beta = 0.25$. The simulations are initialized with the amplitude functions corresponding to the GH mode obtained in the solution of the BiGlobal EVP, scaled to have a maximum kinetic energy equal to $A = 10^{-10}$.

This cross-verification builds confidence on the integrity of the results obtained by numerical solution of the EVP (3.2)–(3.5). However, instead of embarking upon parametric studies of instability by numerical solution of the partial-derivative EVP or by DNS, the question is addressed next whether it is possible to simplify the full system of equations describing linear stability by a polynomial model analogous with that proposed by Theofilis *et al.* (2003) for the orthogonal case; attention is turned to this issue next.

4. An ODE-based polynomial model for three-dimensional linear disturbances in non-orthogonal stagnation-line flows

The question is now addressed whether global instability of incompressible non-orthogonal stagnation line flow can be described by a model which takes into account the potentially existing polynomial nature of the leading eigenmodes along the chordwise spatial direction. Models expanding the eigenmodes of non-orthogonal flow into polynomials of the chordwise coordinate have been employed in an *ad hoc* manner by Floryan (1992) in incompressible and by Lasseigne & Jackson (1992) in compressible non-orthogonal stagnation line flow, while Brattkus & Davis (1991)

	Present work	Lasseigne & Jackson (1992)	Floryan (1992)
Ansatz	$\exp(\mathrm{i}(\beta z - \Omega t))$	$\exp\left(\mathrm{i}\left(a\beta z + a^2\omega t\right)\right)$	$\sin(\beta z)\exp(\sigma t)$
Im [*eigenvalue*]	Ω_i	$a^2\omega/Re$	σ
Re [*eigenvalue*]	Ω_r	0	0
Wavenumber	β	$a\beta$	β
Eigenfunction	Not scaled	Scaled with α	Not scaled

TABLE 3. Scalings of the present ODE system compared with alternatives in the literature.

and Theofilis *et al.* (2003), respectively, showed that local and global stability of orthogonal incompressible flow can be described by a polynomial model reducing the stability problem to a system of ODEs. Guided by the latter work, the amplitude functions of three-dimensional disturbances are assumed to take the form

$$\boldsymbol{Q}_p(x, y) = \sum_{k=0}^{\infty} \hat{\boldsymbol{q}}_k(y)\, x^k, \tag{4.1}$$

where $\hat{\boldsymbol{q}}_k(y) = \left(\hat{u}, \hat{v}, \hat{w}, \hat{p}\right)(y)$ is the vector of one-dimensional disturbance amplitude functions.

Substituting (4.1) into the incompressible continuity and Navier–Stokes equations and linearizing around the basic flow (2.3) the following system of equations for an arbitrary order $K \geqslant 1$ is obtained:

$$(k+1)\,\hat{u}_{k+1} + \hat{v}_k' + \mathrm{i}\,\beta\,\hat{w}_k = 0, \tag{4.2}$$

$$-Re\,\hat{p}_{k+1} + (k+2)(k+1)\,\hat{u}_{k+2} + \left(\mathscr{L} + \mathrm{i}\,Re\,\Omega - (k+1)f'\right)\hat{u}_k - \theta_k f''\,\hat{v}_{k-1} - \left((k+1)\,g'\hat{u}_{k+1} + g''\hat{v}_k\right) = 0, \tag{4.3}$$

$$-Re\,\hat{p}_k' + h_k(k+2)(k+1)\,\hat{v}_{k+2} + h_k\left(\mathscr{L} + \mathrm{i}\,Re\,\Omega - (k-1)f'\right)\hat{v}_k - h_k(k+1)\,g'\hat{v}_{k+1} = 0, \tag{4.4}$$

$$-\mathrm{i}\,Re\,\beta\,\hat{p}_k + h_k(k+2)(k+1)\,\hat{w}_{k+2} + h_k\left(\mathscr{L} + \mathrm{i}\,Re\,\Omega - k\,f'\right)\hat{w}_k - h_k\,Re\,\overline{w}'\hat{v}_k - h_k(k+1)\;\;g'\hat{w}_{k+1} = 0, \tag{4.5}$$

where $\mathscr{L} = \mathscr{D}^2 + f\mathscr{D} - \beta^2 - \mathrm{i}\,\beta\,Re\,\overline{w}$, $\mathscr{D} = \mathrm{d}/\mathrm{d}y$, $\mathscr{D}^2 = \mathrm{d}^2/\mathrm{d}dy^2$, $\theta_0 = 0$, $\theta_k = 1\ (\forall k \geqslant 1)$, $h_0 = 1$ and $h_k = k\ (\forall k \geqslant 1)$.

Model equations for the disturbances in the non-orthogonal case proposed in the past in the literature can be recovered as particular cases of (4.2)–(4.5). For clarity, the Ansatz and scalings used in the present case and in the other two related works in the literature are summarized in table 3. First, in order to compare with Lasseigne & Jackson (1992) in the limit of zero Mach number, a low chordwise polynomial order must be considered. Concretely, using $k = 0$ in (4.2), (4.4) and (4.5) and $k = 1$ in (4.3), one obtains

$$\hat{u}_1 + \hat{v}_0' + \mathrm{i}\,\beta\,\hat{w}_0 = 0, \tag{4.6}$$

$$0 = \hat{v}_1' + \mathrm{i}\,\beta\,\hat{w}_1, \tag{4.7}$$

$$\left(\mathscr{L} + \mathrm{i}\,Re\,\Omega - f'\right)\hat{u}_0 = g'\hat{u}_1 + g''\hat{v}_0 + Re\,\hat{p}_1, \tag{4.8}$$

$$\left(\mathscr{L} + \mathrm{i}\,Re\,\Omega - 2\,f'\right)\hat{u}_1 - f''\hat{v}_0 = g''\hat{v}_1, \tag{4.9}$$

$$\left(\mathscr{L} + \mathrm{i}\,Re\,\Omega + f'\right)\hat{\xi}_0 = g'\hat{\xi}_1 + g''\hat{w}_1 + i\beta Re\,\overline{w}'\hat{w}_0 + Re\mathscr{S}\hat{v}_0, \tag{4.10}$$

$$0 = (\mathscr{L} + \mathrm{i}\,Re\,\Omega)\,\hat{\xi}_1 - \mathrm{i}\beta Re\,\overline{w}'\hat{w}_1 - Re\mathscr{S}\hat{v}_1, \tag{4.11}$$

where $\mathscr{S} = \left(\overline{w}'' + \overline{w}'\,\mathscr{D}\right)$. The first two equations correspond to the mass conservation equation, the following two are the x-momentum conservation and the last two equations are the vorticity equations obtained from the y- and z-momentum equations, with $\hat{\xi}_k = -\mathrm{i}\,\beta\hat{v}_k + \hat{w}_k'$. Note that, although this system is not closed due to the presence of $\hat{v}_1$ and $\hat{w}_1$, Lasseigne & Jackson (1992) have based their analyses on system (4.6)–(4.11), with all terms on the right-hand side taken equal to zero. The degree to which this hypothesis is valid in the incompressible limit is examined in what follows by reference to the global instability analysis results.

Floryan (1992) used the GH model in the non-orthogonal plane stagnation flow in order to model the functional dependence of the perturbations with the chordwise direction. This model is equivalent to that proposed by Lasseigne & Jackson (1992) in the limit of zero Mach number and to the model described in (4.6)–(4.11) when all of the terms on the right-hand side, corresponding to higher truncation orders, are neglected. Both Floryan (1992) and Lasseigne & Jackson (1992) considered real eigenvalues only, corresponding to stationary perturbations. This hypothesis was based on the earlier work of Wilson & Gladwell (1978) on the stability of plane orthogonal stagnation flows which predicted that, owing to the absence of a sweep component in the basic flow, the leading instability was stationary. By taking Ω to be complex in the present case, the leading instability eigenmode is permitted to have non-zero frequency.

Finally the extended Görtler–Hämmerlin model for three-dimensional disturbances described by Theofilis *et al.* (2003) is recovered directly from (4.2)–(4.5) in the limit at $\alpha = \pi/2$,

$$(k+1)\,\hat{u}_{k+1} + \hat{v}_k' + \mathrm{i}\,\beta\,\hat{w}_k = 0, \tag{4.12a}$$

$$-Re\,\hat{p}_{k+1} + (k+2)\,(k+1)\,\hat{u}_{k+2} + \left(\mathscr{L} + \mathrm{i}\,Re\,\Omega - (k+1)f'\right)\hat{u}_k - \theta_k f''\,\hat{v}_{k-1} = 0 \tag{4.12b}$$

$$-Re\,\hat{p}_k' - h_k\,(k+2)\,(k+1)\,\hat{v}_{k+2} + h_k\left(\mathscr{L} + \mathrm{i}\,Re\,\Omega - (k-1)f'\right)\hat{v}_k = 0 \tag{4.12c}$$

$$-\mathrm{i}\,Re\beta\hat{p}_k + h_k\,(k+2)\,(k+1)\,\hat{w}_{k+2} + h_k\left(\mathscr{L} + \mathrm{i}\,Re\,\Omega - kf'\right)\hat{w}_k - h_k\,Re\,\overline{w}'\hat{v}_k = 0. \tag{4.12d}$$

Further, in the orthogonal case two families of solutions can be identified: symmetric solutions, for even powers of $\hat{p}$, and antisymmetric solutions, for odd powers of $\hat{p}$, as described by Theofilis *et al.* (2003). This classification is no longer valid in the non-orthogonal case, and all powers must be included in the expansion for all variables. The first concern is to demonstrate convergence of the above series with k. Convergence of this expansion for the disturbances was demonstrated by Theofilis *et al.* (2003) in the orthogonal case, where three-dimensional disturbances were classified in symmetric and antisymmetric families. Some aspects must be taken into account when choosing the truncation order of the series. The lower-order coefficients depend on the higher-order coefficients at any given truncation order. Consequently, the truncation of expansion (4.1) is only justified if the coefficients associated with the terms neglected are effectively negligible numerically, compared with those retained. Finally, it should be remarked that the truncation of the system of equations (4.12) does not correspond exactly to the system of equations considered by Theofilis *et al.* (2003). In the latter case, the truncation order is taken so that the number of equations

Truncation order, K	GH		A1	
	c_r	$c_i(\times 10^2)$	c_r	$c_i(\times 10^2)$
0	0.3568818305	0.48279122	—	—
1	0.3578462058	0.57797198	0.3554227537	0.21141593
2	0.3578462058	0.57797198	0.3573506523	0.40070171
3	0.3578462057	0.57797198	0.3573506519	0.40070172
4	0.3578462063	0.57797197	0.3573506523	0.40070171
(3.2)–(3.5)	0.3578462113	0.57797207	0.3573489537	0.40053579

TABLE 4. Effect of truncation order of the convergence of the solution of the one-dimensional EVP (4.2)–(4.5) for $\alpha = 70°$, $Re = 775.0$ and $\beta = 0.245$.

is equal to the number of variables for the corresponding symmetric or antisymmetric case, while in the present work a single system of equations is solved.

Table 4 shows the eigenvalues c corresponding to the eigenmodes GH and A1, obtained as solutions of system (4.2)–(4.5) for different truncation orders, compared with the solution of the BiGlobal EVP at $\alpha = 70°$, $Re = 775.0$ and $\beta = 0.245$. The results show that the GH eigenvalue is converged up to the seventh decimal place when the series are truncated at order $K = 1$, highlighting the approximately linear dependence of the disturbance shapes on the x-direction. In addition, as GH mode is nearly symmetric, the truncation at order $K = 0$ already delivers a good approximation to the eigenvalue. The opposite happens when considering the A1 eigenmode, for which the truncation at $K = 0$ does not deliver a physical eigenvalue; the truncation at order $K = 1$ delivers an eigenvalue converged up to the second decimal place; and the eigenvalue for the truncation at $K = 2$ is accurate up to the fourth decimal place.

Figure 6 shows the relative contribution of each polynomial term on the total kinetic energy of the GH mode at $Re = 775$, $\beta = 0.245$ and $\alpha = 70°$. Scaling the amplitudes for the $k = 0$ (x-independent) contribution to be equal to one, the contribution of term $k = 1$ responsible for the linear dependence is $O(10^{-5})$. Contributions of higher-order terms are below 10^{-12}. This observation suggests that even while the polynomial expansion (4.1) cannot be reduced exactly to a linear function, the truncation at $K = 1$ already accounts for most of the physical behaviour and delivers consistent linear stability results.

The question addressed next is whether a change of α has an effect on the qualitative and quantitative agreement between the numerical solutions of the full global linear stability EVP (3.2)–(3.5) and those obtained by solving the model EVP (4.2)–(4.5). Results of the respective systems are obtained at different α values, keeping the pair of (Re, β) parameters constant. Out of several such comparisons made, a representative result is shown in figure 7. On the basis of this and analogous results not presented here the following conclusions may be drawn. First, the very good agreement shown earlier at a given angle α between numerical solutions of the full and the reduced EVP is maintained when the angle α is changed. Second, the hierarchy of leading eigenmodes known from the orthogonal flow is also present when the angle α is varied; the non-orthogonal analogue of the GH mode is always the dominant eigenmode. Third, a given spanwise wavenumber/wavelength at a given Reynolds number experiences amplification beyond that of the orthogonal flow as the angle α is reduced from 90°, while all modes are stabilized below a certain

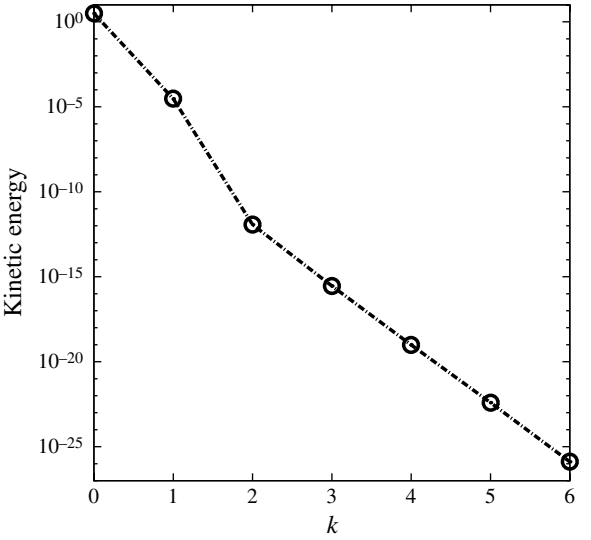

FIGURE 6. Kinetic energy of the polynomial term, $K_k = \left(\hat{u}_k^2 + \hat{v}_k^2 + \hat{w}_k^2\right)/2$, of the GH mode for $\alpha = 70°$, $Re = 775.0$, $\beta = 0.245$ and 64 CGL nodes. Energy was scaled to unity.

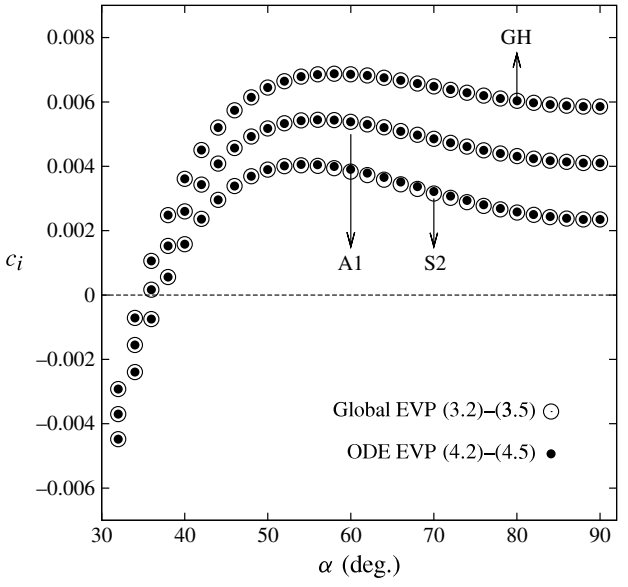

FIGURE 7. Amplification rate c_i of the leading eigenmodes against α at $Re = 800$ and $\beta = 0.255$.

value of α; in the concrete example shown the maximum amplification rate at a fixed $(Re = 800, \beta = 0.255)$ is obtained at $\alpha_{max} \approx 58.16°$, while at this (Re, β) parameter combination the flow is found to be linearly stable below $\alpha \approx 34.1°$.

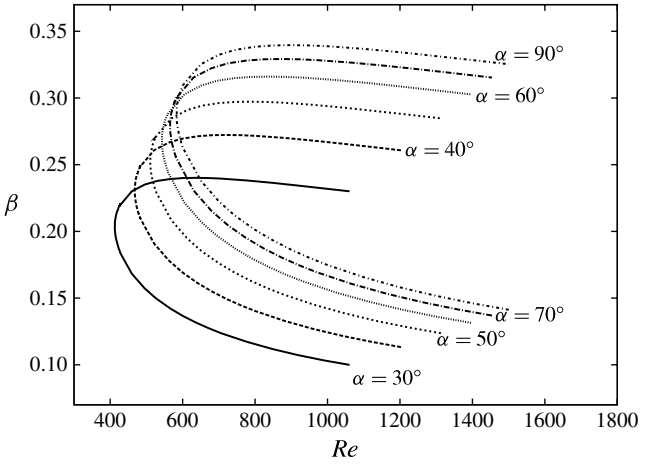

FIGURE 8. Neutral curves of non-orthogonal stagnation-line flow. Curves correspond, from right to left, to $\alpha = 90°$ (10°) 30°.

α (deg.)	Global EVP		ODE $K = 1$		ODE $K = 4$	
	Re_c	β_c	Re_c	β_c	Re_c	β_c
90	583.36	0.287	583.10	0.286	583.10	0.286
80	578.55	0.285	578.65	0.284	578.55	0.285
70	565.35	0.278	565.24	0.277	565.35	0.278
60	542.89	0.266	542.64	0.266	542.89	0.266
50	510.41	0.251	510.35	0.250	510.38	0.252
40	467.71	0.229	467.50	0.229	467.48	0.230
30	412.41	0.203	412.31	0.202	412.45	0.202

TABLE 5. Dependence of the critical parameters (Re, β) on the angle α. The results of BiGlobal EVP and ODE systems with truncation orders $K = 1$ and $K = 4$ are shown.

4.1. *The effect of α on the neutral curves and critical conditions*

Exploiting the agreement between numerical solutions of systems (3.2)–(3.5) and (4.2)–(4.5) the neutral curves of non-orthogonal flow are obtained by focusing on the latter system and the leading GH eigenmode; the results, calculated with 48 CGL nodes and steps of $\Delta Re = 0.5$ and $\Delta\beta = 0.001$ in the Reynolds and wavenumber parameters respectively, are shown in figure 8. Linear interpolation between these results yields the critical parameters shown in table 5. This table compares the critical parameters obtained as the solution of the ODE system (4.2)–(4.5) for the truncation orders $K = 1$ and $K = 4$, with those obtained by solving the BiGlobal EVP. The excellent agreement in all cases strengthens the statement that the ODE model (4.2)–(4.5) at a reasonable truncation level, $K = 1$, suffices to deliver accurate predictions for the leading eigenmode and the critical conditions of non-orthogonal flow.

A second conclusion that can be drawn from these results is that a decrease of the angle α (an increase of *AoA*) has a destabilizing effect on the flow. At the same time, increasingly longer-wavelength perturbations become unstable as the angle α decreases (*AoA* increases).

4.2. *The α-independent linear critical conditions*

The previous discussion is completed by paying closer attention to the trends observed regarding the dependence of the critical parameters on α as its value is decreased from the orthogonal flow. Concretely, a simple relation is sought relating the critical parameters at a given value of α (or AoA) with those of orthogonal flow. In § 2 a formulation for the non-orthogonal stagnation flow was given that, through the introduction of the scaled wall-normal variable $\eta = ay$, delivers an α-independent set of equations. Using this formulation, the three components of velocity can be written as

$$U(x, \eta) = 1/Re\, xa^2 F'(\eta) + 1/Re\, \cos(\alpha)/a\, H(\eta), \tag{4.13}$$

$$V(\eta) = -1/Re\, aF(\eta), \tag{4.14}$$

$$W(\eta) = E(\eta). \tag{4.15}$$

On the other hand, the results presented in § 4.1 show that the linear expansion of the disturbances along the x-direction

$$\boldsymbol{Q}_p(x, \eta) = \hat{\boldsymbol{q}}_0(\eta) + \delta \hat{\boldsymbol{q}}_1(\eta) x \tag{4.16}$$

suffices to capture accurately the leading eigenvalue. Coefficient δ is a parameter that will be determined when matching terms in the disturbance equations, as follows.

Introducing (4.13)–(4.15) and (4.16) in the linearized Navier–Stokes equations, collecting terms on different powers of x, and defining $\delta = a$, one arrives at the following system.

Continuity equation:

$$\times(x^0):\ \hat{u}_1 + \hat{v}_0' + \mathrm{i}\tilde{\beta}\tilde{Re}\,\hat{w}_0 = 0, \tag{4.17}$$

$$\times(x^1):\ \hat{w}_1 = 0, \tag{4.18}$$

x-momentum equation:

$$\times(x^0):\ (\tilde{\mathscr{L}} + F')\hat{u}_0 = -\cos(\alpha)/a^2 H\hat{u}_1 - \tilde{Re}\hat{p}_1 - \cos(\alpha)/a^2 H'\hat{v}_0, \tag{4.19}$$

$$\times(x^1):\ (\tilde{\mathscr{L}} + 2F')\hat{u}_1 + F''\hat{v}_0 = 0, \tag{4.20}$$

$$\times(x^2):\ \hat{v}_1 = 0 \tag{4.21}$$

y-momentum equation:

$$\times(x^0):\ (\tilde{\mathscr{L}} - F')\hat{v}_0 + \tilde{Re}\hat{p}_0' = -\cos(\alpha)/a^2 H\hat{v}_1, \tag{4.22}$$

$$\times(x^1):\ \tilde{\mathscr{L}}\hat{v}_1 + \tilde{Re}\,\hat{p}_1 = 0 \tag{4.23}$$

z-momentum equation:

$$\times(x^0):\ \tilde{\mathscr{L}}\hat{w}_0 + \tilde{Re}E'\hat{v}_0 + \mathrm{i}\tilde{\beta}\tilde{Re}\hat{p}_0 = -\cos(\alpha)/a^2 H\hat{w}_1, \tag{4.24}$$

$$\times(x^1):\ \tilde{\mathscr{L}}\hat{w}_1 + \tilde{Re}\,E'\hat{v}_1 + \mathrm{i}\tilde{\beta}\tilde{Re}\hat{p}_1 = 0. \tag{4.25}$$

In the previous system of ODEs, primes denote differentiation with respect to η and $\tilde{\mathscr{L}} = -\mathrm{i}\tilde{\Omega}\tilde{Re} - F\partial/\partial\eta + \mathrm{i}E\tilde{\beta}\tilde{Re} - \partial^2/\partial\eta^2 + \tilde{\beta}^2$. The new variables $\tilde{Re} = Re/a$, $\tilde{\beta} = \beta/a$ and $\tilde{\Omega} = \Omega/a$ have been introduced in order to obtain a system of equations analogous to (4.6)–(4.11) but in which the angle α does not appear explicitly in the terms on the left-hand side. The only terms that depend on α are those of the form $\cos(\alpha)/a^2$, and are negligible if $\alpha \to \pi/2$. Moreover, from the system of equations

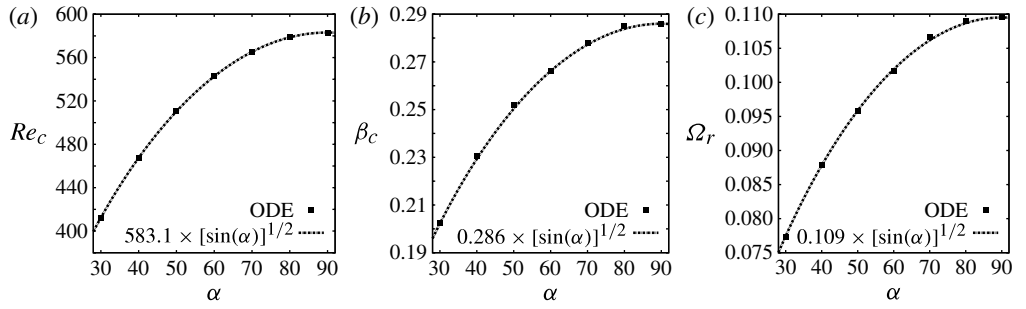

FIGURE 9. Critical Reynolds and β numbers versus α: (*a*) critical Reynolds number versus α; (*b*) critical β number versus α; (*c*) critical frequency, Ω_r, versus α.

it follows that $\hat{v}_1 = \hat{w}_1 = \hat{p}_1 = 0$, resulting in all of the terms on the right-hand side vanishing and leading to a system of equations for the disturbances analogous with that used by Lasseigne & Jackson (1992).

The main result of this derivation is that the linear instability results in non-orthogonal flow, corresponding to the leading GH mode, can be recovered accurately using an α-independent system of equations with parameters $\tilde{Re}$ and $\tilde{\beta}$, and then scaled to the corresponding physical values of Re and β. In particular, the critical conditions, e.g. critical Reynolds number Re_c, critical spanwise wavenumber β_c and critical frequency Ω_{cr} for any non-orthogonal case defined by α, can be obtained directly from the results for the orthogonal stagnation line flow by

$$Re_c(\alpha) = Re_c(\alpha = \pi/2)\sqrt{\sin\alpha} \approx 583.1\ \sqrt{\sin\alpha}, \tag{4.26a}$$

$$\beta_c(\alpha) = \beta_c(\alpha = \pi/2)\sqrt{\sin\alpha} \approx 0.286\ \sqrt{\sin\alpha}, \tag{4.26b}$$

$$\Omega_{r,c}(\alpha) = \Omega_{r,c}(\alpha = \pi/2)\sqrt{\sin\alpha} \approx 0.109\ \sqrt{\sin\alpha}. \tag{4.26c}$$

Figure 9 compares the critical conditions as a function of α shown in table 5, with the theoretical scaling (4.26), showing a very good agreement. It should be remarked that in the previous derivations within this section it was assumed that the angle α is close to $\pi/2$; however, the present results show that the proposed scaling holds true for a wide range of angles. Another interesting consequence is that all of the eigenvalues presented as $c = \Omega/\beta$ (figure 3 and tables 2 and 4) do not depend directly on α and are valid for different angles as far as the values of $\tilde{Re}$ and $\tilde{\beta}$ are preserved.

5. Summary

Linear stability analysis of the non-orthogonal incompressible attachment-line boundary-layer flow has been investigated. A combination of two-dimensional non-orthogonal basic flow (proposed by Stuart (1959), Tamada (1979) and Dorrepaal (1986)) and swept boundary-layer flow was considered as basic flow. BiGlobal stability analysis, in which no assumptions with respect to the symmetry of the perturbations have been made, was performed and delivered results in very good agreement with those obtained by independently performed DNSs.

A polynomial model in the spirit of analogous work in the orthogonal limit (Theofilis *et al.* 2003) but without assumption on the solution symmetries has been proposed in order to describe the leading eigenmodes, generalizing those of earlier analyses (Floryan 1992; Lasseigne & Jackson 1992) its results being justified by

comparison with those of global instability analysis and DNS. The polynomial model transforms the PDE-based global EVP into an ODE-based EVP, the results of which were shown to agree very well with those of the more general methodologies. The computational efficiency advantage offered by the ODE-based model, permitted calculating the neutral curves of non-orthogonal flow at several values of $0 < \alpha \leqslant \pi/2$ ($0 \leqslant AoA < \pi/2$). As was done in earlier work in an *ad hoc* manner, the critical conditions of non-orthogonal flow were related to those of orthogonal flow via a simple algebraic transformation; the present work provided the missing justification in the incompressible regime by reference to global linear instability and DNS results.

Present results show that a decrease in α (an increase in AoA) from the orthogonal case leads to a linear destabilization of the flow. This observation might raise the question of the validity of the results as $\alpha \to 0$. In this paper, the STD non-orthogonal attachment-line flow model, that verifies the Navier–Stokes equations for all α, is taken as a canonical flow field. Identification of the canonical model with a particular application and its corresponding α value is beyond the scope of this paper. In this regard, the experimental data obtained by (Poll 1979) in the case of orthogonal flow is the only known confirmation that the swept Hiemenz model to which the STD model reduces at $\alpha = \pi/2$ is relevant to the attachment-line application. Further experimental efforts are desirable in this respect.

Acknowledgements

Support from the Spanish Ministry of Science and Innovation through Grant MICINN-TRA2009-13648: *'Metodologías computacionales para la predicción de inestabilidades globales hidrodinámicas y aeroacústicas de flujos complejos'* is gratefully acknowledged. The work of D.R. was partially funded by the Marie Curie COFUND programme.

REFERENCES

AMESTOY, P. R., DUFF, I. S., L'EXCELLENT, J.-Y. & KOSTER, J. 2001 A fully asynchronous multifrontal solver using distributed dynamic scheduling. *SIAM J. Matrix Anal. Applics* **1**, 15–41.

BERTOLOTTI, F. P. 1999 On the connection between cross-flow vortices and attachment-line instabilities. In *Proc. of the IUTAM Laminar-Turbulent Symposium V* (ed. W. Saric & H. Fasel), pp. 625–630, Sedona.

BRATTKUS, K. & DAVIS, S. H. 1991 The linear stability of plane stagnation-point flow against general disturbances. *Q. J. Mech. Appl. Maths* **44** (2), 135–146.

COLLIS, S. & LELE, S. 1999 Receptivity to surface roughness near a swept leading edge. *J. Fluid Mech.* **380**, 141–168.

CRIMINALE, W. O., JACKSON, T. L. & LASSEIGNE, D. G. 1994 Evolution of disturbances in stagnation-point flow. *J. Fluid Mech.* **270**, 331–347.

CROUCH, J. D., GARBARUK, A. & MAGIDOV, D. 2007 Predicting the onset of flow unsteadiness based on global instability. *J. Comput. Phys.* **224** (2), 924–940.

DORREPAAL, J. M. 1986 An exact solution of the Navier–Stokes equations which describes non-orthogonal stagnation-point flow in two dimensions. *J. Fluid Mech.* **163**, 141–147.

FLORYAN, J. 1992 Stability of plane nonorthogonal stagnation flow. *AIAA J.* **30** (6), 1659–1662.

FLORYAN, J. M. & DALLMANN, U. C. 1990 Flow over a leading edge with distributed roughness. *J. Fluid Mech.* **216**, 629–656.

GASTER, M. 1967 On the flow along swept leading edges. *Aero. Q.* **18**, 165–184.

GÖRTLER, H. 1955 Dreidimensionale Instabilität der ebenen Staupunktströmung gegenüber wirbelartigen Störungen. In *50 Jahre Grenzschichtforschung* (ed. H. Görtler & W. Tollmien). pp. 304–314. Vieweg und Sohn.

GRAY, W. E. 1952 The effect of wing sweep on laminar flow. *Royal Aircraft Establishment, RAE TM* 255 (*ARC* 14, 929).

GUÉGAN, A., SCHMID, P. J. & HUERRE, P. 2008 Spatial optimal disturbances in swept attachment-line boundary layers. *J. Fluid Mech.* **603**, 179–188.

HALL, P., MALIK, M. R. & POLL, D. I. A. 1984 On the stability of an infinitive swept attachment line boundary layer. *Proc. R. Soc. Lond.* A **395**, 229–245.

HÄMMERLIN, H. 1955 Zur Instabilitätstheorie der ebenen Staupunktströmung. In *50 jahre grenzschichtforschung*, pp. 315–327. Vieweg und Sohn.

HIEMENZ, K. 1911 Die Grenzschicht an einem in den gleichförmigen Flüssigkeitsstrom eingetauchten geraden Kreiszylinder. *Dingl. Polytechn. J.* **326**, 321–324, thesis, Göttingen.

JOSLIN, R. D. 1996 Simulation of nonlinear instabilities in an attachment-line boundary layer. *Fluid Dyn. Res.* **18** (2), 81–97.

LASSEIGNE, D. G. & JACKSON, T. L. 1992 Stability of a non-orthogonal stagnation flow for three-dimensional disturbances. *Theor. Comput. Fluid Dyn.* **3**, 207–218.

LASSEIGNE, D. G., JACKSON, T. L. & HU, F. Q. 1992 Temperature and suction effects on the instability of an infinite swept attachment line. *Phys. Fluids* A **4** (9), 2008–2012.

LIN, R. S. & MALIK, M. R. 1996 On the stability of attachment-line boundary layers. Part 1. The incompressible swept Hiemenz flow. *J. Fluid Mech.* **311**, 239–255.

LIN, R. S. & MALIK, M. R. 1997 On the stability of attachment-line boundary layers. Part 2. The effect of leading-edge curvature. *J. Fluid Mech.* **333**, 125–137.

LUNDBLADH, A., SCHMID, P., BERLIN, S. & HENNINGSON, D. 1994 Simulation of by-pass transition in spatially evolving flow. In *Proceedings of the AGARD Symposium on Application of Direct and Large Eddy Simulation to Transition and Turbulence*, no. CP-551 in AGARD, pp. 18.1–18.13.

LYELL, M. J. & HUERRE, P. 1985 Linear and nonlinear stability of plane stagnation flow. *J. Fluid Mech.* **161**, 295–312.

MACK, C. J. & SCHMID, P. J. 2010 Direct numerical study of hypersonic flow about a swept parabolic body. *Comput. Fluids* **39** (10), 1932–1943.

MACK, C. J., SCHMID, P. J. & SESTERHENN, J. 2008 Global stability of swept flow around a parabolic body: connecting attachment-line and crossflow modes. *J. Fluid Mech.* **611**, 205–214.

OBRIST, D. 2000 On the stability of the swept leading-edge boundary layer. PhD thesis, University of Washington.

OBRIST, D. & SCHMID, P. J. 2003 On the linear stability of swept attachment-line boundary layer flow. Part 2. Non-modal effects and receptivity. *J. Fluid Mech.* **493**, 31–58.

PÉREZ, J. M. 2012 Efficient numerical methods for global linear instability. Analysis and modeling of non-orthogonal swept attachment-line boundary layer flow. PhD thesis, School of Aeronautics, Technical University of Madrid.

PFENNINGER, W. & BACON, J. 1969 *Amplified Laminar Boundary Layer Oscillation and Transition at the Attachment Line of a 45° Swept Flat-nosed Wing with and without Suction*. Plenum.

POLL, D. I. A. 1979 Transition in the infinite swept attachment line boundary layer. *Aero. Q.* **30**, 607–629.

RODRÍGUEZ, D. & THEOFILIS, V. 2010 Structural changes of laminar separation bubbles induced by global linear instability. *J. Fluid Mech.* **655**, 280–305.

ROSENHEAD, L. 1963 *Laminar Boundary Layers*. Oxford University Press.

SCHLICHTING, H. 1979 *Boundary Layer Theory*, 7th edn. McGraw-Hill.

SPALART, P. R. 1988 Direct numerical study of leading-edge contamination. *AGARD-CP*-438 **5**, 1–13.

STUART, J. T. 1959 The viscous flow near a stagnation point when the external flow has uniform vorticity. *J. Aero/Space Sci.* **26**, 124–125.

SUTERA, S. P. 1965 Vorticity amplification in stagnation point flow and its effects on heat transfer. *J. Fluid Mech.* **21** (3), 513–534.

TAMADA, K. 1979 Two-dimensional stagnation-point flow impinging obliquely on a plane wall. *J. Phys. Soc. Japan* **46**, 310–311.

THEOFILIS, V. 1993 Numerical experiments on the stability of leading edge boundary layer flow: a two-dimensional linear study. *Intl J. Numer. Meth. Fluids* **16**, 153–170.

THEOFILIS, V. 1995 Spatial stability of incompressible attachment-line flow. *Theor. Comp. Fluid Dyn.* **7** (3), 159–171.

THEOFILIS, V. 2003 Advances in global linear instability of nonparallel and three-dimensional flows. *Prog. Aerosp. Sci.* **39** (4), 249–315.

THEOFILIS, V. 2011 Global linear instability. *Annu. Rev. Fluid Mech.* **43**, 319–352.

THEOFILIS, V., FEDOROV, A. & COLLIS, S. 2006 Leading-edge boundary layer flow (Prandtl's vision, current developments and future perspectives). In *IUTAM Symposium on One Hundred Years of Boundary Layer Research* **129**, 73–82.

THEOFILIS, V., FEDOROV, A., OBRIST, D. & DALLMANN, U. C. 2003 The extended Görtler–Hämmerlin model for linear instability of three-dimensional incompressible swept attachment-line boundary layer flow. *J. Fluid Mech.* **487**, 271–313.

WILSON, S. & GLADWELL, I. 1978 The stability of a two-dimensional stagnation flow to three-dimensional disturbances. *J. Fluid Mech.* **84**, 517–527.

XIONG, Z. & LELE, S. 2007 Stagnation-point flow under free stream turbulence. *J. Fluid Mech.* **590**, 1–33.